Academic Journal of Science and Technology
ISSN: 2771-3032 | Vol. 23, No. 2, 2026

Sensorless Control of a Permanent-Magnet Synchronous Motor Based on Incremental Deadbeat Predictive Current Control and an Adaptive Sliding-Mode Observer

Guoqing Xiang, Xiao Zeng*, Liang Zheng

School of Mechanical Engineering, Xihua University, Chengdu 610039, China
* Corresponding author: Xiao Zeng (Email: zengxiao@mail.xhu.edu.cn)

Abstract: To address the strong dependence of conventional deadbeat predictive current control on motor parameters and the effect of observation errors on rotor-angle estimation during sensorless operation, this paper investigates a permanent-magnet synchronous motor (PMSM) control method that combines incremental deadbeat predictive current control with an adaptive sliding-mode observer. First, an incremental predictive model is derived by taking the difference between the discrete current equations of two consecutive sampling periods, thereby reducing the influence of parameter mismatches in the permanent-magnet flux linkage and stator resistance on predictive control. In addition, the one-sampling-period delay inherent in digital control is taken into account, and compensating voltage commands are generated using historical current and voltage information. Subsequently, a sliding-mode observer based on adaptive back-electromotive-force estimation and a phase-locked loop is designed, and its stability is analyzed using a Lyapunov-based approach. Simulation results show that, under the permanent-magnet flux-linkage and stator-resistance mismatch conditions considered in this study, the proposed incremental deadbeat predictive current control achieves a smaller steady-state q-axis current deviation than conventional deadbeat predictive current control. Under the specified speed-tracking and sudden-load-application conditions, the adaptive sliding-mode observer exhibits lower speed ripple and a smaller steady-state rotor-angle estimation error than the conventional sliding-mode observer, while its estimated speed tracks the actual motor speed more closely.

Keywords: Permanent Magnet Synchronous Motor; Incremental Deadbeat Predictive Current Control; Sliding-mode Observer.

1. Introduction

Permanent Magnet Synchronous Motors (PMSM) have been widely used in new-energy vehicles, medical equipment, and industrial drives because of their simple structure, low operating noise, high reliability, and high power factor [1]. Among the various types of electric machines, Surface-mounted Permanent Magnet Synchronous Motors (SPMSM) offer significant advantages, including a relatively high power factor, simple construction, and good operational reliability [2].

The Proportional Integral (PI) controller has been widely employed in permanent magnet synchronous motor (PMSM) control systems owing to its simple structure, low implementation cost, and relatively straightforward parameter tuning [3]. However, PMSMs are inherently complex controlled plants characterized by multiple variables, strong coupling, nonlinearities, and time-varying parameters. In practical operation, the system performance is also susceptible to parameter variations, load disturbances, and other uncertain factors, which may consequently degrade the control accuracy and dynamic performance. The effectiveness of conventional PI controllers relies, to a certain extent, on the proper tuning of both system and controller parameters. Therefore, under complex operating conditions, conventional PI control still exhibits certain limitations in terms of dynamic response, disturbance rejection capability, and adaptability to parameter variations [4]. Among the existing current-loop control strategies, Deadbeat Predictive Current Control (DPCC) has attracted considerable attention from researchers worldwide because of its fast dynamic response, relatively simple control structure, and suitability for digital implementation [5].

Although DPCC provides good dynamic performance, its control effectiveness is relatively sensitive to the accuracy of the motor-model parameters [6].When parameters such as the stator resistance, inductance, and permanent-magnet flux linkage are mismatched, discrepancies arise between the predictive model and the actual motor, thereby producing current-prediction errors [7]. In [8], Incremental Deadbeat Predictive Current Control (IDPCC) was proposed. This method uses difference operations between two adjacent control periods to predict the voltage increment, thereby eliminating the effects of the permanent-magnet flux-linkage and stator-resistance parameters.

Accurate estimation of rotor position and speed is a fundamental prerequisite for achieving high-performance control of PMSM. In particular, under the field-oriented control (FOC) strategy, precise estimation of rotor position and speed is of great significance to the dynamic response, operational stability, and control accuracy of the motor control system [9]. At present, typical PMSM control systems still commonly employ mechanical position sensors to obtain rotor-position information [10]. However, conventional position sensors typically require relatively complex mechanical mounting structures and associated electrical circuits. Under extremely complex operating conditions, their reliability and stability may be compromised, thereby

increasing the risk of system failures and adversely affecting the operational stability of PMSM speed regulation systems. In contrast, sensorless control technology enables the indirect estimation of rotor position and speed information by establishing appropriate mathematical models and state-observation algorithms, eliminating the need for additional mechanical position-detection devices. This approach effectively reduces hardware complexity as well as installation and maintenance costs, while enhancing the adaptability of the motor to complex operating environments. Therefore, sensorless control technology has significant research value and has attracted widespread attention [11].

Sensorless control estimates rotor states using measurable quantities such as voltage and current, thereby reducing dependence on mechanical position sensors. Early research in this field primarily focused on induction motors and was subsequently extended to PMSM. Depending on their underlying principles and applicable speed ranges, sensorless control methods can generally be classified into two categories: model-based methods, which are primarily applicable to medium- and high-speed operating regions, and methods based on rotor saliency effects, which are mainly suitable for low- and zero-speed operation [12]. In recent years, extensive research has been conducted by scholars worldwide to address the limitations of conventional sliding mode observers (SMO) in rotor position and speed estimation, including relatively large estimation errors and pronounced high-frequency chattering induced by sliding-mode switching. These studies aim to further improve the estimation performance and operational stability of sensorless control systems, the authors of [13] designed a nonsingular fast terminal sliding surface and introduced a sliding-mode control law with an integral term, thereby effectively improving the estimation accuracy of the observer. In [14], a sinusoidal saturation function with an adjustable boundary layer was used to replace the conventional switching function. Its performance was compared with those of elementary, terminal sliding-mode, and hyperbolic-tangent saturation functions to mitigate chattering in the sliding-mode observer.

To address the chattering and phase-lag problems associated with conventional sliding-mode observers, this paper develops an adaptive sliding-mode observer (ASMO) that combines a back-EMF estimator with a phase-locked loop (PLL). The adaptive back-EMF estimation stage is used to extract back-EMF information, thereby avoiding phase lag in the estimated electrical angle and improving the observation accuracy. The PLL is less affected by bandwidth limitations, which improves observer performance and accelerates the tracking response of the system. In addition, a saturation function and a variable sliding-mode gain are employed to effectively suppress chattering. The two sliding-mode observers are compared through simulations and experiments. The results demonstrate that the adaptive sliding-mode observer provides improved performance over the conventional sliding-mode observer and exhibits superior operating characteristics.

2. Mathematical Model of Permanent Magnet Synchronous Motor

The SPMSM is investigated in this study. For an SPMSM, *Ld*=*Lq*. Therefore, the voltage equations in the d–q rotating reference frame can be expressed as follows:

$$\begin{cases} u_d = Ri_d + L_d \frac{\mathrm{d}}{\mathrm{d}t} i_d - \omega_e L_q i_q \\ u_q = Ri_q + L_q \frac{\mathrm{d}}{\mathrm{d}t} i_q + \omega_e \left(L_d i_d + \psi_f\right) \end{cases} \tag{1}$$

The electromagnetic torque equation is expressed as follows:

$$T_e = \frac{3}{2} p_n \psi_f i_q \tag{2}$$

The mechanical motion equation is expressed as follows:

$$J \frac{d\omega_m}{dt} = T_e - T_L - B\omega_m \tag{3}$$

where *Ls* is the stator inductance in the d- and q-axes; *id* and *iq* are the d and q-axis stator currents, respectively; *ud* and *uq* are the d- and q-axis stator voltages, respectively; *Rs* is the stator resistance; *We* is the rotor electrical angular velocity; *Pn* is the number of pole pairs; ψ_f is the permanent magnet flux linkage; *Wm* is the mechanical angular velocity; *J* is the moment of inertia; *TL* is the load torque; and *B* is the viscous damping coefficient.

3. Deadbeat Predictive Current Control

3.1. Conventional Desadbeat Predictive Current Control

By applying the first-order forward Euler method to discretize Equation (1), the discrete-time stator voltage equations of the PMSM in the d–q reference frame can be obtained as follows:

$$\begin{cases} u_d(k) = R_s i_d(k) + L_s \frac{i_d(k+1) - i_d(k)}{T_s} - \omega_e(k) L_s i_q(k) \\ u_q(k) = R_s i_q(k) + L_s \frac{i_q(k+1) - i_q(k)}{T_s} + \omega_e(k) L_s i_d(k) + \omega_e(k) \psi_f \end{cases} \tag{4}$$

$u_d(k)$ and $u_q(k)$ denotes the reference value of the stator voltage in the d-q reference frame at the k-th sampling instant.; $i_d(k)$ and $i_q(k)$ denotes the actual sampled value of the stator current at the k-th sampling instant. $i_d(k+1)$ and $i_q(k+1)$ denotes the actual sampled value of the stator current at the (k+1)-th sampling instant; T_s denotes the control period of the system; $\omega_e(k)$ denotes the measured rotor electrical angle at sampling instant k. By setting $i_d^*(k) = i_d(k+1)$ and $i_q^*(k) = i_q(k+1)$ in (4), where $i_d^*(k)$ and $i_q^*(k)$ represent the reference currents in the d-and q-axis, respectively, at sampling instant k, the reference voltages $u_d^*(k)$ and $u_q^*(k)$ in the d-q reference frame can be expressed as follows:

$$\begin{cases} u_d^*(k) = R_s i_d(k) + L_s \frac{i_d^*(k) - i_d(k)}{T_s} - \omega_e(k) L_s i_q(k) \\ u_q^*(k) = R_s i_q(k) + L_s \frac{i_q^*(k) - i_q(k)}{T_s} + \omega_e(k) L_s i_d(k) + \omega_e(k) \psi_f \end{cases} \tag{5}$$

In an ideal DPCC system, it is assumed that the digital controller has sufficiently high computational speed so that current sampling, analog-to-digital (A/D) conversion, control algorithm execution, and pulse-width modulation (PWM) updating can all be completed within a single control period. Consequently, the calculated control voltage can be applied to the motor in a timely manner, enabling the actual current to

track its reference value at the next sampling instant. However, in practical digital control systems, owing to the processing time required for A/D conversion, control algorithm execution, and PWM duty-cycle calculation, the PWM signals generated during the current control period are typically transferred to shadow registers and do not take effect until the next update event. As a result, an inherent one-sampling-period delay exists between current sampling and the actual application of the voltage vector to the inverter, thereby adversely affecting the real-time performance and control accuracy of current tracking. To compensate for the one-step delay associated with the application of the reference voltage command $u^*(k)$, calculated at sampling instant k but updated at sampling instant k+1, the current at sampling instant k+1 should first be predicted at sampling instant k. Subsequently, the predicted current is used to calculate the reference voltage command $u^*(k+1)$, which can be expressed as follows:

$$\begin{cases} u_d^*(k+1) = R_s i_d(k+1) + L_s \frac{i_d(k+2)-i_d(k+1)}{T_s} - \omega_e(k+1) L_s i_q(k+1) \\ u_q^*(k+1) = R_s i_q(k+1) + L_s \frac{i_q(k+2)-i_q(k+1)}{T_s} + \omega_e(k+1) L_s i_d(k+1) + \omega_e(k+1)\psi_f \end{cases} \tag{6}$$

where $u_d^*(k+1)$ and $u_q^*(k+1)$ denote the reference voltage commands for the d- and q-axes -axes, respectively, at sampling instant k+1.

According to (6), the feedback current $i(k+2)$ can only track the reference current $i^*(k)$ at sampling instant k+2. Therefore, the reference current $i^*(k)$ at sampling instant k is set equal to the feedback current $i(k+2)$ at sampling instant k+2, $i_d^*(k) = i_d(k+2)$ and $i_q^*(k) = i_q(k+2)$. However, $\omega_e(k+1)$ and $i(k+1)$ are unknown quantities that cannot be directly obtained at sampling instant k. Since the control period is sufficiently short and the mechanical time constant of the motor is much larger than its electrical time constant, the rotor electrical angular velocities at two consecutive sampling instants can be assumed to be approximately equal, $\omega_e(k+1) \approx \omega_e(k)$. Meanwhile, the unknown currents $i_d(k+1)$ and $i_q(k+1)$ need to be predicted at sampling instant k, which can be expressed as follows:

$$\begin{cases} i_d^p(k+1) = \left(1 - \frac{R_s T_s}{L_s}\right) i_d(k) + T_s \omega_e(k) i_q(k) + \frac{T_s}{L_s} u_d^*(k) \\ i_q^p(k+1) = \left(1 - \frac{R_s T_s}{L_s}\right) i_q(k) - T_s \omega_e(k) i_d(k) + \frac{T_s}{L_s} u_q^*(k) - \frac{T_s}{L_s}\psi_f \omega_e(k) \end{cases} \tag{7}$$

where $i_d^p(k+1)$ and $i_q^p(k+1)$ denote the predicted d-q axis currents at sampling instant k+1, respectively. By substituting $i_d^*(k) = i_d(k+2)$, $i_q^*(k) = i_q(k+2)$, and $\omega_e(k+1) \approx \omega_e(k)$ into (3) and combining the resulting equation with (4), the predicted reference voltage commands at sampling instant k+1 can be obtained as follows:

$$\begin{cases} u_d^*(k+1) = R_s i_d^p(k+1) + L_s \frac{i_d^*(k)-i_d^p(k+1)}{T_s} - \omega_e(k) L_s i_q^p(k+1) \\ u_q^*(k+1) = R_s i_q^p(k+1) + L_s \frac{i_q^*(k)-i_q^p(k+1)}{T_s} + \omega_e(k) L_s i_d^p(k+1) + \omega_e(k)\psi_f \end{cases} \tag{8}$$

where $u_d^*(k+1)$ and $u_q^*(k+1)$ denote the predicted reference voltage commands for the d-q axis, respectively, at sampling instant k+1.

3.2. Incremental Deadbeat Predictive Current Control

The incremental model can eliminate the steady-state current error caused by flux linkage mismatch in DPCC. The predicted currents of the incremental DPCC at sampling instant k+1 can be expressed as follows:

$$\begin{cases} \Delta i_d^{\mathrm{pre}}(k+1) = \left(1 - \frac{T_s \Delta R}{L_s}\right) \Delta i_d(k) + T_s \omega_e(k) \Delta i_q(k) + \\ \qquad \frac{T_s}{L_s} \Delta u_d(k); \\ \Delta i_q^{\mathrm{pre}}(k+1) = \left(1 - \frac{T_s \Delta R}{L_s}\right) \Delta i_q(k) - T_s \omega_e(k) \Delta i_d(k) + \\ \qquad \frac{T_s}{L_s} \Delta u_q(k)。 \end{cases} \tag{9}$$

By adding the current increment to the current at the present sampling instant, the flux-linkage parameter can be eliminated, yielding the predicted current at the (k+1) th sampling instant as follows:

$$\begin{cases} i_d^{\mathrm{pre}}(k+1) = i_d(k) + \left(1 - \frac{T_s \Delta R}{L_s}\right) \Delta i_d(k) + \\ \qquad T_s \omega_e(k) \Delta i_q(k) + \frac{T_s}{L_s} \Delta u_d(k); \\ i_q^{\mathrm{pre}}(k+1) = i_q(k) + \left(1 - \frac{T_s \Delta R}{L_s}\right) \Delta i_q(k) - \\ \qquad T_s \omega_e(k) \Delta i_d(k) + \frac{T_s}{L_s} \Delta u_q(k)。 \end{cases} \tag{10}$$

where the estimated voltage increment is given by:

$$\begin{cases} \Delta u_d^{\mathrm{ref}}(k+1) = \frac{L_s}{T_s} [\Delta i_d^{\mathrm{ref}}(k) - \Delta i_d^{\mathrm{pre}}(k+1)] + \\ \qquad \Delta R \Delta i_d^{\mathrm{pre}}(k+1) - L_s \omega_e(k) \Delta i_q^{\mathrm{pre}}(k+1); \\ \Delta u_q^{\mathrm{ref}}(k+1) = \frac{L_s}{T_s} [\Delta i_q^{\mathrm{ref}}(k) - \Delta i_q^{\mathrm{pre}}(k+1)] + \\ \qquad \Delta R \Delta i_q^{\mathrm{pre}}(k+1) + L_s \omega_e(k) \Delta i_d^{\mathrm{pre}}(k+1)。 \end{cases} \tag{11}$$

It can be concluded from the above derivation that IDPCC eliminates the flux-linkage parameter from the predictive model, thereby mitigating the degradation in control performance and the deterioration in prediction accuracy caused by variations in flux linkage.

4. Sliding Mode Observer Design

4.1. Design of the Conventional Sliding Mode Observer

The SMO is primarily employed to estimate the disturbance term in the motor model, namely the back electromotive force (back-EMF). In this paper, an SMO based on the extended electromotive force (EEMF) model is developed to estimate the rotor speed and position. The mathematical model of the motor in the stationary $\alpha-\beta$ reference frame can be expressed as follows:

$$\begin{bmatrix} u_\alpha \\ u_\beta \end{bmatrix} = \begin{bmatrix} R_s + pL_d & (L_d - L_q)\omega_r \\ -(L_d - L_q)\omega_r & R_s + pL_d \end{bmatrix} \begin{bmatrix} i_\alpha \\ i_\beta \end{bmatrix} + E_{\text{ex}} \begin{bmatrix} -\sin\theta_r \\ \cos\theta_r \end{bmatrix} \quad (12)$$

Where E_{ex} denotes the extended electromotive force, which is expressed as follows:

$$E_{\text{ex}} = \omega_r \lambda_f = (L_d - L_q)(\omega_r i_d - p i_q) + \omega_r \psi_f \quad (13)$$

For a surface-mounted permanent magnet synchronous motor (SPMSM), the extended electromotive force expression in (13) simplifies to a quantity that depends only on the rotor speed. The magnitude of the back-EMF increases with the rotor speed and decreases as the speed decreases. The voltage equations can then be rewritten in the current state-space form as follows:

$$\frac{\mathrm{d}}{\mathrm{d}t}\begin{bmatrix} i_\alpha \\ i_\beta \end{bmatrix} = \frac{1}{L_d}\begin{bmatrix} -R & -(L_d - L_q)\omega_e \\ (L_d - L_q)\omega_e & -R \end{bmatrix}\begin{bmatrix} i_\alpha \\ i_\beta \end{bmatrix} + \frac{1}{L_d}\begin{bmatrix} u_\alpha \\ u_\beta \end{bmatrix} - \frac{1}{L_d}\begin{bmatrix} E_\alpha \\ E_\beta \end{bmatrix} \quad (14)$$

To obtain the estimated extended electromotive force, the conventional sliding mode observer is typically designed as follows:

$$\frac{\mathrm{d}}{\mathrm{d}t}\begin{bmatrix} \hat{i}_\alpha \\ \hat{i}_\beta \end{bmatrix} = \frac{1}{L_d}\begin{bmatrix} -R & -(L_d - L_q)\omega_e \\ (L_d - L_q)\omega_e & -R \end{bmatrix}\begin{bmatrix} \hat{i}_\alpha \\ \hat{i}_\beta \end{bmatrix} + \frac{1}{L_d}\begin{bmatrix} u_\alpha \\ u_\beta \end{bmatrix} - \frac{1}{L_d}\begin{bmatrix} v_\alpha \\ v_\beta \end{bmatrix} \quad (15)$$

where $\hat{\imath}_\alpha$ and $\hat{\imath}_\beta$ denote the estimated stator currents, while u_α and u_β represent the control inputs of the observer.

By taking the difference between (14) and (15), the stator current estimation error dynamics can be derived as follows:

$$\frac{\mathrm{d}}{\mathrm{d}t}\begin{bmatrix} \tilde{\imath}_\alpha \\ \tilde{\imath}_\beta \end{bmatrix} = \frac{1}{L_d}\begin{bmatrix} -R & -(L_d - L_q)\omega_e \\ (L_d - L_q)\omega_e & -R \end{bmatrix}\begin{bmatrix} \tilde{\imath}_\alpha \\ \tilde{\imath}_\beta \end{bmatrix} + \frac{1}{L_d}\begin{bmatrix} E_\alpha - v_\alpha \\ E_\beta - v_\beta \end{bmatrix} \quad (16)$$

where $\tilde{\imath}_a = \hat{\imath}_a - i_a$ and $\tilde{\imath}_\beta = \hat{\imath}_\beta - i_\beta$ denote the stator current estimation errors. The sliding mode control law is designed as follows:

$$\begin{bmatrix} v_\alpha \\ v_\beta \end{bmatrix} = \begin{bmatrix} k\,\mathrm{sgn}(\hat{\imath}_\alpha - i_\alpha) \\ k\,\mathrm{sgn}(\hat{\imath}_\beta - i_\beta) \end{bmatrix} \quad (17)$$

Once the observer state variables reach the sliding surface and satisfy $\lambda=0$ and $i_p=0$, Once the observer states reach and remain on the sliding surface, according to the principle of sliding-mode control, the control input required to maintain the system states on the sliding surface can be regarded as the equivalent control input, which yields:

$$\begin{bmatrix} E_\alpha \\ E_\beta \end{bmatrix} = \begin{bmatrix} v_\alpha \\ v_\beta \end{bmatrix}_{\text{eq}} = \begin{bmatrix} k\,\mathrm{sgn}(\tilde{\imath}_\alpha)_{\text{eq}} \\ k\,\mathrm{sgn}(\tilde{\imath}_\beta)_{\text{eq}} \end{bmatrix} \quad (18)$$

4.2. Design of the Adaptive Sliding Mode Observer

The current equations in the stationary reference frame can be rewritten as follows:

$$\frac{\mathrm{d}}{\mathrm{d}t} i_s = \mathrm{A} i_s + \mathrm{B} u_s + \mathrm{K}_e E_s \quad (19)$$

$$\mathbf{A} = \begin{bmatrix} -\frac{R}{L_s} & 0 \\ 0 & -\frac{R}{L_s} \end{bmatrix}; \mathbf{B} = \begin{bmatrix} -\frac{1}{L_s} & 0 \\ 0 & -\frac{1}{L_s} \end{bmatrix}; \mathbf{K}_e = \begin{bmatrix} -\frac{1}{L_s} & 0 \\ 0 & -\frac{1}{L_s} \end{bmatrix}; u_s = [u_\alpha \quad u_\beta]^{\mathrm{T}}; i_s = [i_\alpha \quad i_\beta]^{\mathrm{T}}; E_s = [E_\alpha \quad E_\beta]^{\mathrm{T}}$$

Where i_s denotes the stator current, u_s denotes the stator voltage, and E_s represents the back electromotive force, which satisfies the following relationship:

$$E_s = \begin{bmatrix} -\psi_f \omega_e \sin\theta_e \\ \psi_f \omega_e \cos\theta_e \end{bmatrix} \quad (20)$$

Furthermore, the differential equation of the back electromotive force E_s is given by:

$$\dot{E}_s = \frac{\mathrm{d}}{\mathrm{d}t}\begin{bmatrix} -\psi_f \omega_e \sin\theta_e \\ \psi_f \omega_e \cos\theta_e \end{bmatrix} = \omega_e \begin{bmatrix} -\psi_f \omega_e \cos\theta_e \\ -\psi_f \omega_e \sin\theta_e \end{bmatrix} = \omega_e \begin{bmatrix} -E_\beta \\ E_\alpha \end{bmatrix} \quad (21)$$

To design the sliding mode observer, the sliding surface is first defined as follows:

$$s = \tilde{\imath}_s = \hat{\imath}_s - i_s = [\tilde{\imath}_\alpha \quad \tilde{\imath}_\beta]^{\mathrm{T}} \quad (22)$$

The adaptive SMO is designed as:

$$\frac{\mathrm{d}}{\mathrm{d}t}\hat{\imath}_s = \mathrm{A}\hat{\imath}_s + \mathrm{B} u_s + \mathrm{K}_e \hat{E}_s + \mathrm{K}\,\mathrm{sign}(s) \quad (23)$$

Where: $\mathbf{K}_e = \begin{bmatrix} k & 0 \\ 0 & k \end{bmatrix}$, kis a constant satisfying the following condition: $k < \min\begin{bmatrix} -\frac{R}{L_s}|\tilde{\imath}_\alpha| - \frac{1}{L_s}|\tilde{E}_\alpha|, \\ -\frac{R}{L_s}|\tilde{\imath}_\beta| - \frac{1}{L_s}|\tilde{E}_\beta| \end{bmatrix}$; $\hat{E}_s = \begin{bmatrix} -\psi_f \hat{\omega}_e \sin\hat{\theta}_e \\ \psi_f \hat{\omega}_e \cos\hat{\theta}_e \end{bmatrix}$.

According to (19) and (23), the current estimation error dynamics can be derived as:

$$\frac{\mathrm{d}}{\mathrm{d}t}\tilde{\imath}_s = \mathbf{A}\tilde{\imath}_s + \mathbf{K}_e \tilde{E}_s + \mathbf{K}\,\mathrm{sign}(s) \quad (24)$$

The adaptation law for the back electromotive force (back-EMF) is designed as follows:

$$\begin{cases} \frac{\mathrm{d}}{\mathrm{d}t}\hat{E}_\alpha = -\hat{\omega}_e\hat{E}_\beta - l\tilde{E}_\alpha \\ \frac{\mathrm{d}}{\mathrm{d}t}\hat{E}_\beta = \hat{\omega}_e\hat{E}_\alpha - l\tilde{E}_\beta \\ \frac{\mathrm{d}}{\mathrm{d}t}\hat{\omega}_e = \tilde{E}_\alpha\hat{E}_\beta - \hat{E}_\alpha\tilde{E}_\beta \end{cases} \quad (25)$$

To verify the stability of the proposed ASMO, a Lyapunov function is defined as follows:

$$V = \frac{1}{2}(\tilde{E}_\alpha{}^2 + \tilde{E}_\beta{}^2 + \tilde{\omega}_e{}^2) \quad (26)$$

Since the mechanical time constant of the motor is generally much larger than its electrical time constant, the rotor speed can be approximated as constant over one estimation period. Accordingly. the adaptive law for the back-EMF can be further derived from (25) as follows:

$$\begin{cases} \frac{\mathrm{d}}{\mathrm{d}t}\tilde{E}_\alpha = -\hat{\omega}_e\hat{E}_\beta + \omega_e E_\beta - l\tilde{E}_\alpha \\ \frac{\mathrm{d}}{\mathrm{d}t}\tilde{E}_\beta = \hat{\omega}_e\hat{E}_\alpha - \omega_e E_\alpha - l\tilde{E}_\beta \\ \frac{\mathrm{d}}{\mathrm{d}t}\tilde{\omega}_e = \tilde{E}_\alpha\hat{E}_\beta - \hat{E}_\alpha\tilde{E}_\beta \end{cases} \quad (27)$$

Substituting (27) into (26) yields:

$$V = \tilde{E}_\alpha\dot{\tilde{E}}_\alpha + \tilde{E}_\beta\dot{\tilde{E}}_\beta + \tilde{\omega}_e\dot{\tilde{\omega}}_e = -l(\tilde{E}_\alpha{}^2 + \tilde{E}_\beta{}^2) \le 0 \quad (28)$$

Equation (28) satisfies the Lyapunov stability criterion, thereby demonstrating the stability of the proposed algorithm.

The adaptive regulation of rotor speed is closely related to variations in back-EMF estimation error. Under steady-state conditions, the estimated extended electromotive force (EEMF) converges to its actual value, thereby effectively reducing the back-EMF estimation error, improving the accuracy of rotor position and speed estimation, and significantly enhancing the overall performance of the sensorless motor control system.

5. Simulation Results and Analysis

5.1. Block Diagram of the Control Model

The PMSM adopts a dual closed-loop vector control strategy, as illustrated in Fig. 1. The feedback currents are processed by the IDPCC to generate the reference voltage commands, which are subsequently applied to the motor through SVPWM. Meanwhile, the three-phase stator currents are fed into the ASMO to estimate the rotor speed and position. These estimated values are then used to replace the measured values, thereby achieving sensorless closed-loop control of the PMSM.

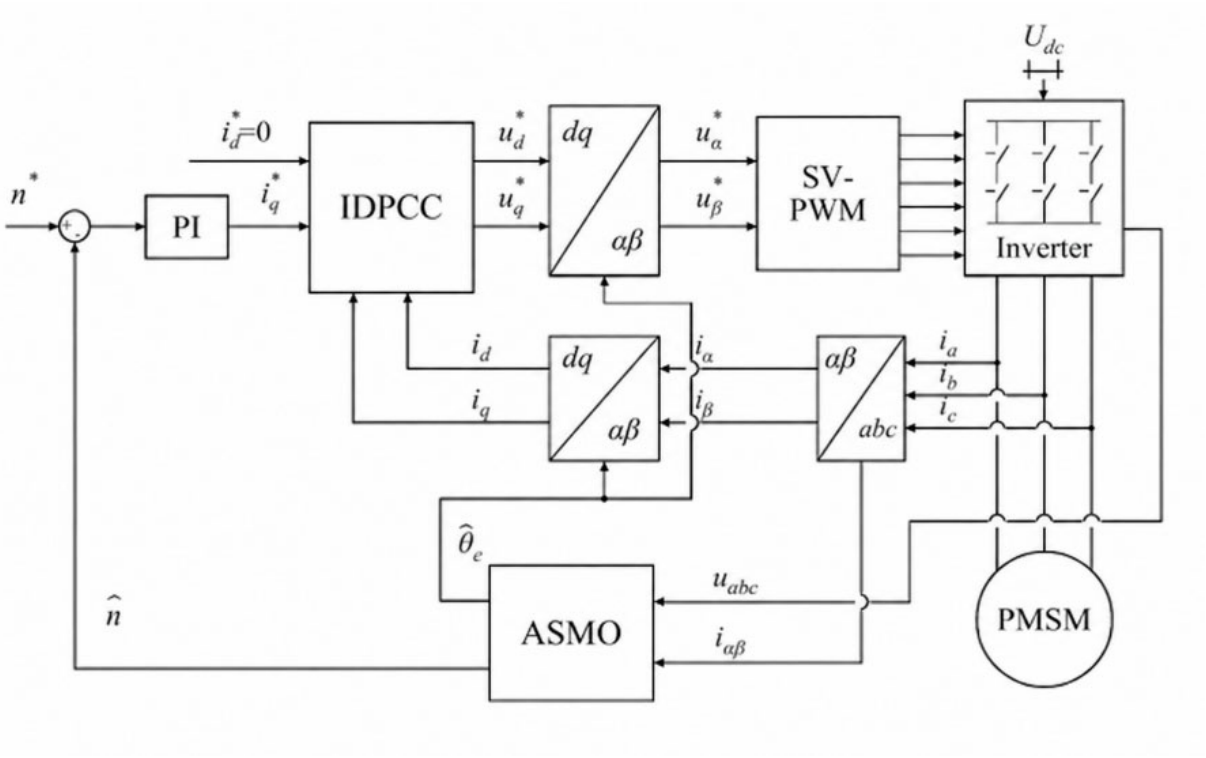


Figure 1. shows the control system block diagram based on IDPCC and ASMO

5.2. Simulation Results

The motor employed in this study is a surface-mounted permanent magnet synchronous motor (SPMSM), whose main parameters are listed in Table I. Based on the proposed control scheme, a corresponding simulation model is established in MATLAB/Simulink. Simulations are conducted under different rotor speeds and load conditions to evaluate the speed tracking performance, rotor position estimation, and corresponding estimation errors. The q-axis current responses under magnetic flux linkage and stator resistance parameter mismatches are illustrated in Fig. 2.

Table 1. Motor parameters

Parameter	value
Number of pole pairs P_n	4
Stator resistance R_s / Ω	0.89
Stator inductance L_s / mH	0.62
Permanent magnet flux linkage ψ_f / Wb	0.00838
Viscous damping coefficient B / (N·m·s/rad)	0.0008
Moment of inertia J / (kg·m^2)	0.000028

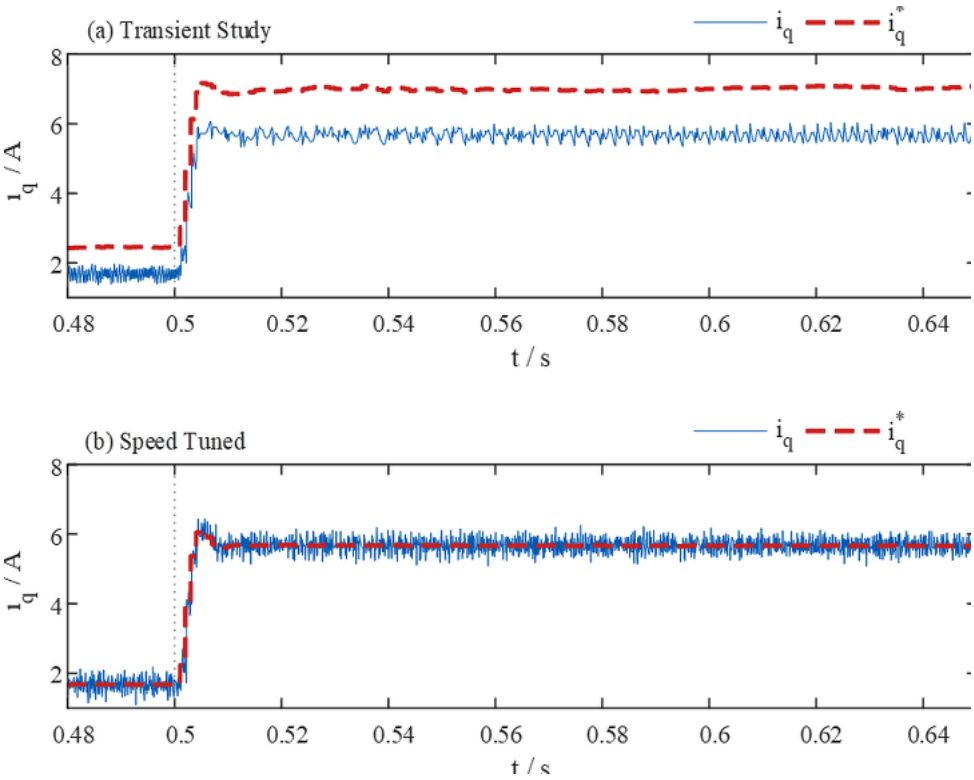
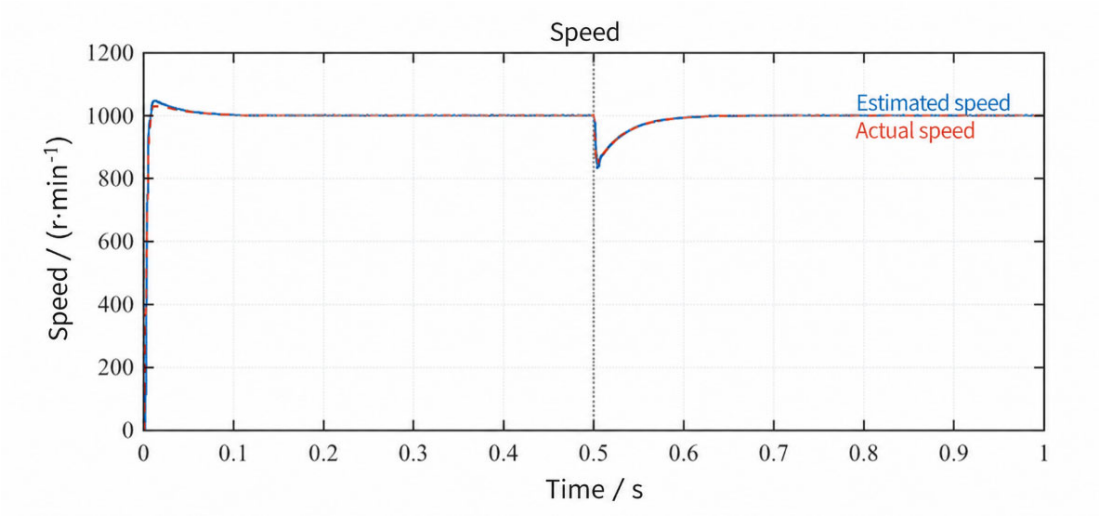


Figure 2. Predicted q-axis current graph

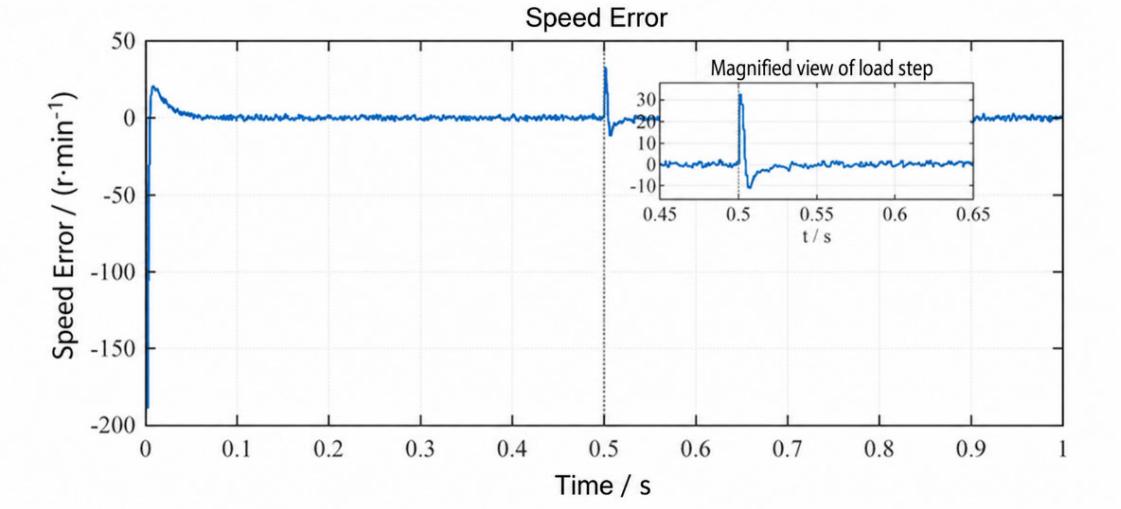
As can be observed from the waveforms, under flux linkage and stator resistance parameter mismatches, the conventional DPCC exhibits a pronounced steady-state offset in the q-axis current, indicating a systematic deviation caused by parameter mismatches. In contrast, the IDPCC significantly reduces this offset while maintaining a fast dynamic response. Consequently, the proposed IDPCC achieves reduced steady-state tracking errors, lower sensitivity to parameter variations, and improved current control accuracy under parameter mismatch conditions.

Based on the developed model, a sensorless SMO is designed, and a comparative study is conducted between the conventional SMO and the ASMO. In the simulation, the reference motor speed is set to 1000 rpm, and a step load torque is applied at 0.5 s to evaluate the dynamic responses of the estimated rotor speed and position. Fig. 3 presents the simulation results obtained using the conventional SMO, whereas Fig. 4 illustrates the corresponding results obtained using the ASMO.

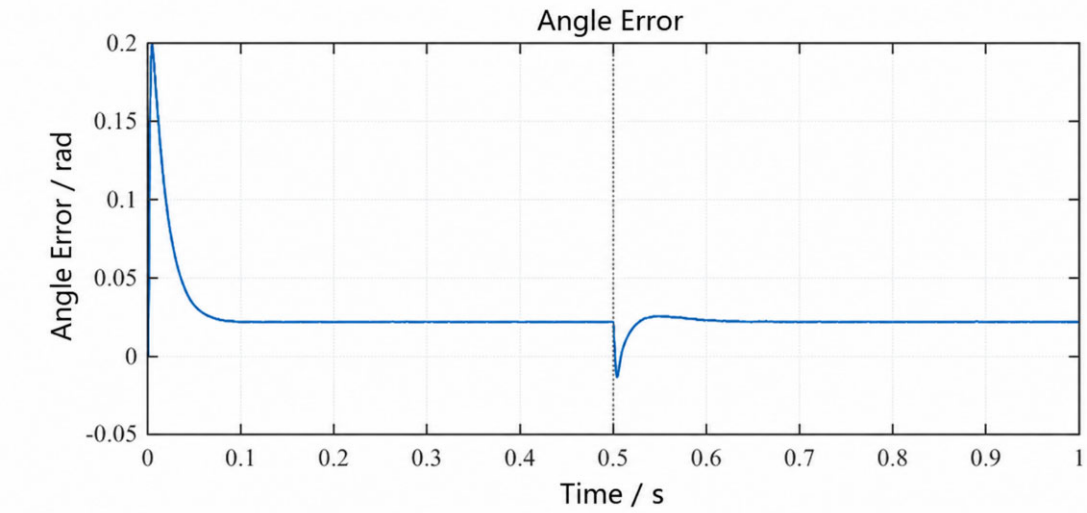
A comparative analysis of the waveforms presented in Figs. 3 and 4 demonstrates the superior estimation performance of the ASMO. As shown in Figs. 3(a) and 4(a), although both observers are capable of tracking the actual rotor speed, the conventional SMO exhibits a noticeable tracking deviation following the sudden load disturbance, whereas the ASMO maintains more accurate speed tracking during the transient process. Regarding the speed estimation error, Fig. 3(b) reveals relatively pronounced periodic oscillations under steady-state conditions. In contrast, the speed estimation error shown in Fig. 4(b) exhibits significantly reduced fluctuations and a smoother response. Furthermore, the rotor position estimation error presented in Fig. 3(c) indicates that the conventional SMO can ensure bounded convergence and stable position estimation; however, a certain steady-state estimation bias remains. As illustrated in Fig. 4(c), the ASMO achieves a smaller steady-state rotor position estimation error, demonstrating an effective reduction in the steady-state bias of rotor position estimation.



(a) Actual Rotor Speed and Estimated Rotor Speed

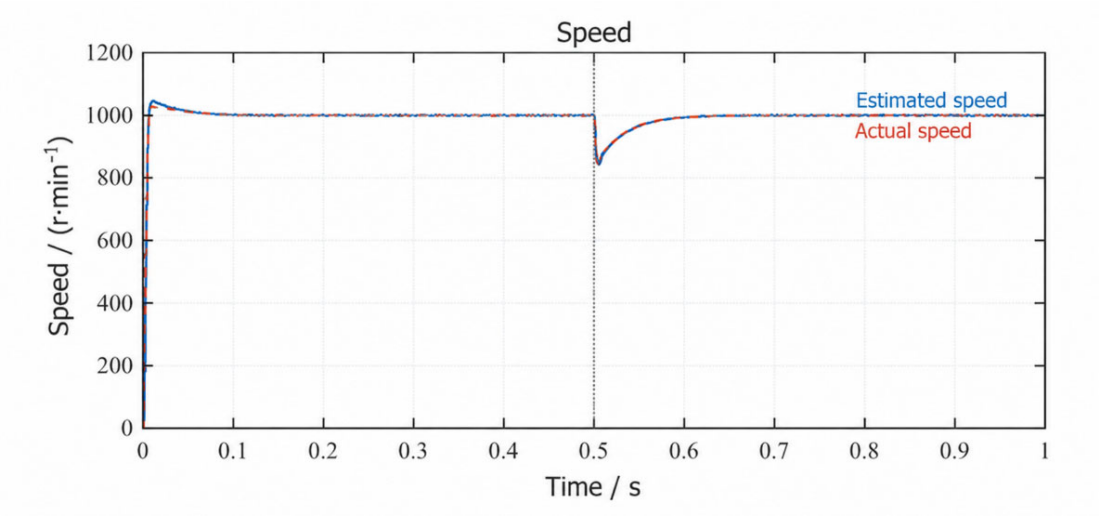


(b) Speed Error

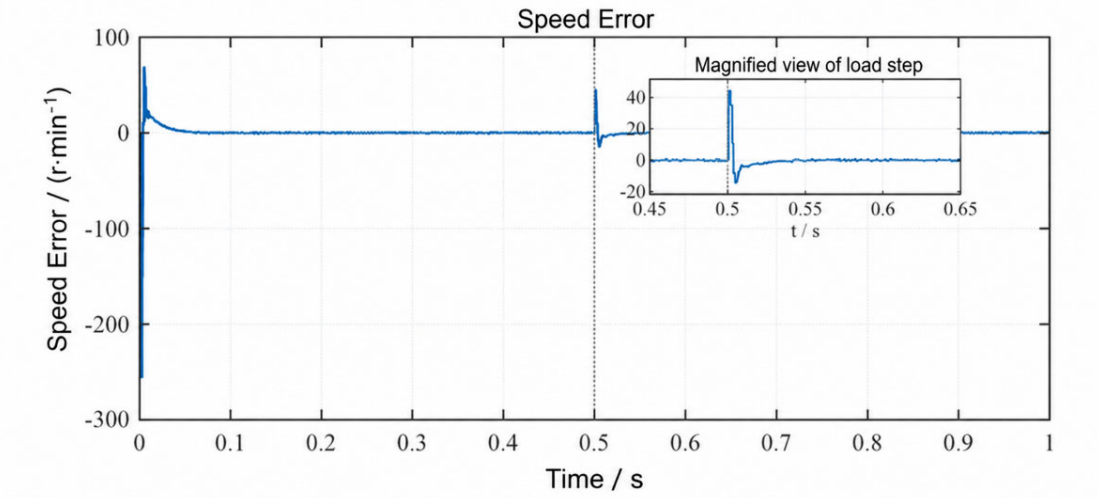


(c) Angle Error

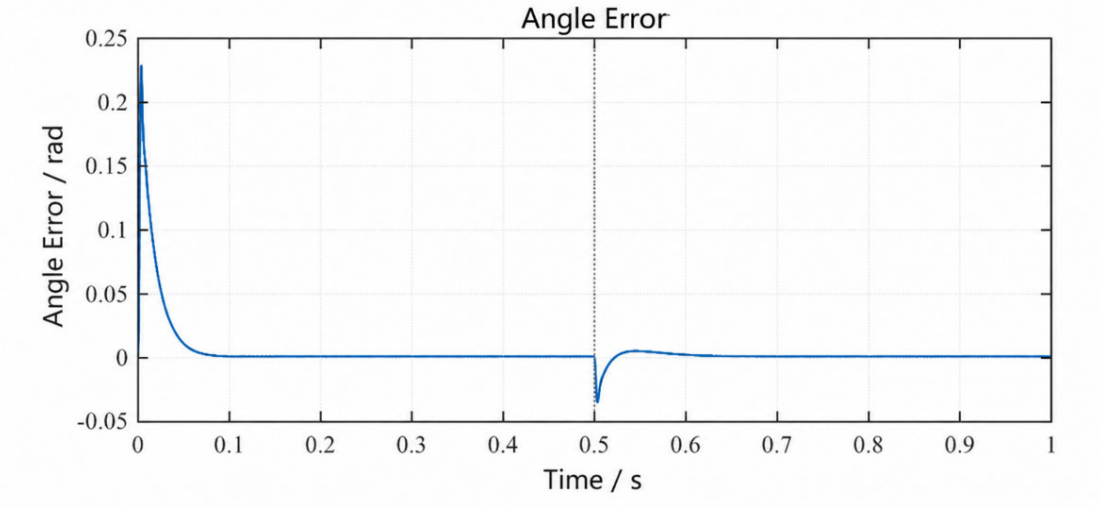
Figure 3. Simulation waveforms of the conventional sliding mode observer



(a) Actual Rotor Speed and Estimated Rotor Speed



(b) Speed Error



(c) Angle Error

Figure 3. Simulation waveforms of the adaptive sliding mode observer

6. Conclusion

This paper addresses the inconsistency between the prediction model and the actual motor dynamics in conventional DPCC under motor parameter mismatches. An IDPCC strategy is developed by constructing an incremental prediction model based on the differences between adjacent sampling periods. Furthermore, historical current and voltage information is utilized to compensate for the one-step delay inherent in digital control systems. According to the theoretical derivations and simulation results, the proposed IDPCC exhibits a smaller steady-state q-axis current error

than conventional DPCC under the specified permanent magnet flux linkage and stator resistance mismatch conditions. These results demonstrate that IDPCC can effectively mitigate the adverse effects of flux linkage and resistance variations on current prediction and tracking performance.

Regarding sensorless control, an adaptive law for back electromotive force estimation is integrated with a phase-locked loop, and the stability of the proposed ASMO is analyzed using a Lyapunov function under the specified assumptions. Compared with the conventional SMO, the proposed ASMO exhibits reduced speed estimation oscillations and smaller steady-state rotor position estimation errors. Moreover, it achieves improved speed tracking accuracy under sudden load disturbances. These results indicate that the proposed ASMO provides favorable dynamic estimation performance and disturbance adaptability under the investigated simulation conditions.

In summary, the proposed IDPCC primarily improves current prediction and control performance under parameter mismatch conditions, while the ASMO enhances rotor speed and position estimation in sensorless FOC systems. By improving the current control and state estimation stages, respectively, the two methods jointly contribute to the overall performance enhancement of the proposed control system. The effectiveness of the proposed methods is supported by the theoretical stability analysis and simulation results.

References

[1] Zhao, X., Wang, H., & Jin, H. (2025). Model predictive current control based on discrete space vector modulation for PMSM. Electric Machines and Control, 29(3), 50–58+73. https://doi.org/10.15938/j.emc.2025.03.005.

[2] Zhang, L., Zhu, X., Gao, J., & et al. (2019). Design and analysis of new five-phase flux-intensifying fault-tolerant interior-permanent-magnet motor for sensorless operation. IEEE Transactions on Industrial Electronics, 67(11), 9338–9347. https://doi.org/10.1109/TIE.2019.2955407

[3] Zhang, Y., Xu, B., Wei, H., & et al. (2023). New model reference adaptive deadbeat predictive current control of PMSM. Electric Machines and Control, 27(9), 157–167. https://doi.org/10.15938/j.emc.2023.09.017

[4] Li, P., Duan, G., Zhang, B., & et al. (2024). Event-triggered control for servo motor systems based on fully actuated system approach and dynamical compensator. IEEE Transactions on Industrial Electronics, 71(12), 15404–15413. https://doi.org/10.1109/TIE.2024.3515273

[5] Chen, B., & Chen, M. (2013). AC speed control systems (3rd ed.). China Machine Press.

[6] Wei, Y., Mao, J., Zhang, C., & et al. (2024). Permanent magnet synchronous motor servo system based on disturbance-rejection-enhanced generalized predictive control. Control and Decision, 39(6), 1967–1976. https://doi.org/10.13195/j.kzyjc.2022.1834

[7] Sun, X., Cao, J., Lei, G., & et al. (2021). A robust deadbeat predictive controller with delay compensation based on composite sliding-mode observer for PMSMs. IEEE Transactions on Power Electronics, 36(9), 10428–10439. https://doi.org/10.1109/TPEL.2021.3063226

[8] Ma, Z., & Kennel, R. (2013). Continuous set nonlinear model predictive control for PMSM drives. 2013 15th European Conference on Power Electronics and Applications (EPE), 1–10. https://doi.org/10.1109/EPE.2013.6631873

[9] Zhang, S., Lei, L., Zhang, C., & et al. (2023). An improved deadbeat predictive current control method for SPMSM drives with a novel adaptive disturbance observer. Journal of Beijing Institute of Technology (English Edition), 32(1), 107–123. https://doi.org/10.15918/j.jbit1004-0579.2022.080

[10] Xu, W. (2025). Research on sensorless vector control technology for permanent magnet synchronous motors over the full speed range [Doctoral dissertation]. Jiangsu University. https://doi.org/10.27170/d.cnki.gjsuu.2025.001586

[11] He, J., Zhang, W., & Zhai, L. (2023). Sensorless model predictive flux control of AFFSPM machine based on improved sliding mode observer. Proceedings of the CSEE, 43(3), 1189–1200. https://doi.org/10.13334/j.0258-8013.pcsee.212463

[12] Gao, X. (2025). Research on sensorless control strategies for permanent magnet synchronous motors based on a sliding mode observer [Doctoral dissertation]. Xiangtan University. https://doi.org/10.27426/d.cnki.gxtdu.2025.001238

[13] Wang, H., Zhao, C., Wan, D., & et al. (2019). Sensorless control of permanent magnet synchronous motor based on nonsingular fast terminal sliding mode observer. Electric Machines & Control Application, 46(1), 28–33.

[14] Lu, X., Lin, H., Feng, Y., & et al. (2015). Soft switching sliding mode observer for PMSM sensorless control. Transactions of China Electrotechnical Society, 30(2), 106–113. https://doi.org/10.19595/j.cnki.1000-6753.tces.2015.02.014